frontiers in Materials

ORIGINAL RESEARCH
published: 14 January 2021
doi: 10.3389/fmats.2020.606092

Dislocation-Controlled Low-Temperature Superplastic Deformation of Ti-6Al-4V Alloy

Chao Liu[1], Xin Wang[1], Ge Zhou[1], Feng Li[1], Siqian Zhang[1], Haoyu Zhang[1], Lijia Chen[1] and Haijian Liu[2]*

[1]School of Materials Science and Engineering, Shenyang University of Technology, Shenyang, China, [2]Shanghai Spaceflight Precision Machinery Institute, Shanghai, China

The superplastic tension and deformation mechanism of Ti-6Al-4V alloy at 923 K and a tensile speed of 10^{-3}, 5×10^{-3}, or 5×10^{-2} s^{-1} was studied on an AG 250KNE electronic tension tester. Through theoretical modeling, the unit dislocation count of this alloy during superplastic deformation was introduced into the Ruano–Wadsworth–Sherby (R-W-S) deformation mechanism map, and a new deformation mechanism map involving dislocation count was plotted. Thereby, the mechanism underling the low-temperature superplastic deformation of this alloy was predicted. It was found the superplastic tension of Ti-6Al-4V at the tested temperature was controlled by dislocation movement, and with an increase in strain rate, the deformation transited from the dislocation-controlled mechanism with a stress index of 4 to the dislocation glide mechanism with a stress index of 5 or 7. At the strain rate of 10^{-3} s^{-1}, this alloy reached the largest tension rate of 790% and strain rate sensitivity index of 0.52 and had excellent low-temperature superplastic properties.

Keywords: Ti-6Al-4V alloy, low-temperature superplasticity, strain rate sensitivity index m, deformation mechanism map, dislocation

OPEN ACCESS

Edited by:
Minghui Cai,
Northeastern University, China

Reviewed by:
Yanbin Jiang,
Central South University, China
Qi Chao,
Deakin University, Australia

****Correspondence:***
Ge Zhou
zhouge@sut.edu.cn

Specialty section:
This article was submitted to Structural Materials, a section of the journal Frontiers in Materials

Received: *14 September 2020*
Accepted: *10 November 2020*
Published: *14 January 2021*

Citation:
Liu C, Wang X, Zhou G, Li F, Zhang S, Zhang H, Chen L and Liu H (2021) Dislocation-Controlled Low-Temperature Superplastic Deformation of Ti-6Al-4V Alloy. Front. Mater. 7:606092. doi: 10.3389/fmats.2020.606092

INTRODUCTION

Ti-6Al-4V alloy, as a typical α+β two-phase titanium alloy, possesses favorable comprehensive properties and thus is widely applied into forming manufacture of complex components in air navigation weapons, equipment, and ships (Vanderhasten et al., 2007; Li et al., 2014; Meng et al., 2016). In recent years, as the overall design performance indices of weapons and equipment are increasingly enhanced, the multilayer structured complex-shape parts are often manufactured via superplastic forming/bonding by diffusion and through one-time near-net-shape forming, based on the designing concept of reinforced rib sandwich structures. To improve the forming precision of complex structured parts, prolong the service life of dies, and lower energy consumption, researchers are interested in how to lower the superplastic forming temperature and control the structural stability of this alloy during superplastic forming while ensuring the feasibility of the superplastic forming process, which becomes hot spots in this field. Thus, the behaviors and mechanism of low-temperature superplastic deformation of Ti-6Al-4V have been studied worldwide.

As for the low-temperature superplasticity of Ti-6Al-4V (Shahmir et al., 2018; Zhang et al., 2018; Zhang et al., 2018; Zhou et al., 2018), Langdon et al. produced nanocrystal grains using high-pressure torsion and obtained a maximum tension rate of 815% at 1073 K. Ding et al. ultrafined cold-rolled Ti-6Al-4V sheets and acquired the maximum tension rate of 820% at 923 K. Cai et al. grain-refined

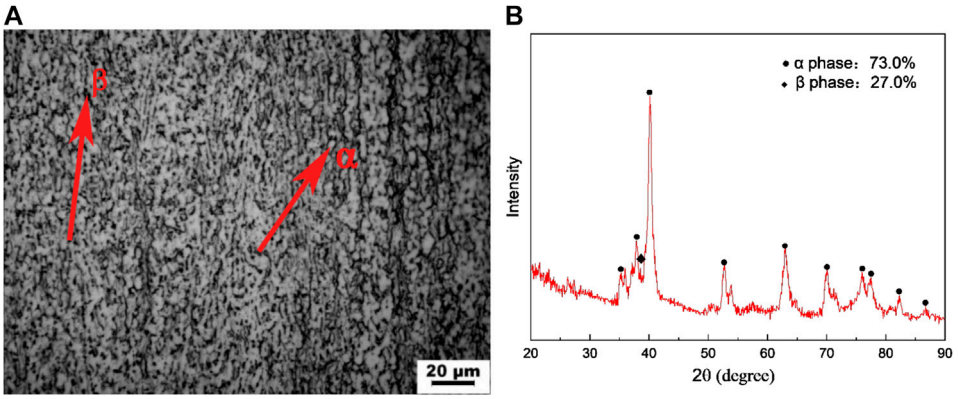

FIGURE 1 | Original structure of Ti-6Al-4V **(A)** OM (500) and **(B)** XRD.

this alloy through stirred friction and maximized the tension rate to 1,130% at 873 K. The above results indicate that the main method of improving low-temperature superplasticity of Ti-6Al-4 V alloy is grain refinement, in which the coordination of grain boundary slip during superplastic deformation is fully utilized. With deformation mechanism maps involving dislocation count, Zhou Ge et al. predicted the superplastic deformation mechanism of Ti-6Al-4 V at 973–1123 K and found the superplastic deformation mechanism transited from grain boundary sliding to dislocation glide (a stress index of 7) and grain boundary slip (a stress index of 4) with a decrease in temperature and observed that the superplastic deformation was modulated by dislocation. Thus, when the superplastic deformation temperature of Ti-6Al-4 V continually dropped while ensuring its elongation above 600%, both the grain boundary slip mechanism and the effects of dislocation on superplasticity should be considered. However, little has been studied about the superplastic deformation behaviors of Ti-6Al-4 V below 973 K, and no study has been conducted about the superplastic deformation of this alloy under the dislocation-controlled mechanism.

In this study, the superplastic tensile behaviors and deformation mechanism of Ti-6Al-4 V alloy at 923 K and different strain rates were studied. The Ruano–Wadsworth–Sherby (R-W-S) deformation mechanism maps involving dislocation count were used to predict the deformation mechanisms under different testing conditions. Together with microstructure characterization by transmission electron microscopy (TEM) and superplastic behaviors as feature parameters, the deformation mechanisms underlying the low-temperature superplastic deformation of this alloy under dislocation control were uncovered. The findings will theoretically support the low-temperature superplastic process optimization of Ti-6Al-4V.

MATERIAL AND METHODS

The studied material Ti-6Al-4V sheet alloy was chemically composed of (wt%) the following: Al, 6.01; V, 3.89; Fe, 0.21; C, 0.04; Ti, bal. Sheets were 2 mm thick and in grain size of 7.6 μm

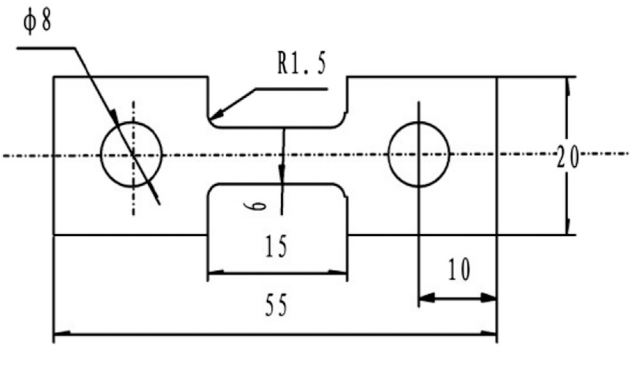

FIGURE 2 | Schematic diagram of tensile specimen dimension (unit: mm).

and consisted of 73% α phase and 27% β phase (**Figure 1**). The Ti-6Al-4V alloy sheets were prepared according to the alloy composition requirements above. Specifically, 4 mm-thick sheets were obtained after vacuum consumable melting and multipass hot rolling and cold rolling. The superplastic tensile specimens were prepared by linear cutting. Tensile specimen dimension is shown in **Figure 2**.

Using an AG 250KNE electronic tension tester, the specimens were heated to 923 K, kept there for 10 min, and then superplastically elongated at a constant crosshead speed and strain rate of 10^{-3}, 5×10^{-3}, or 5×10^{-2} s^{-1}. After water quenching to room temperature, the high-temperature deformed structures were reserved. The whole experiments were conducted under argon gas protection. The microstructures were observed under an OLYMPUS GX51 metallographic microscope, with 6 ml HNO_3+100 ml H_2O+3 ml HF as the etching agent. The α and β phases of specimens under different thermal treatment states were qualitatively analyzed by an XRD-7000 X-ray diffractometer (XRD; Shimadzu, Japan). The structural dislocation and grain

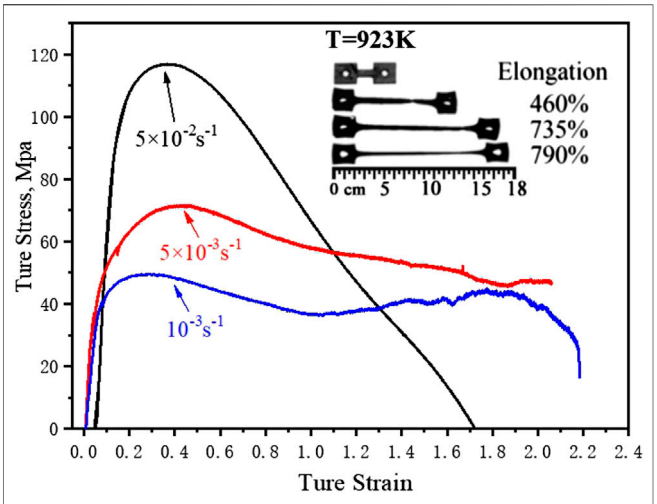

FIGURE 3 | Superplastic tensile stress-strain curves of Ti-6Al-4V (T = 923 K).

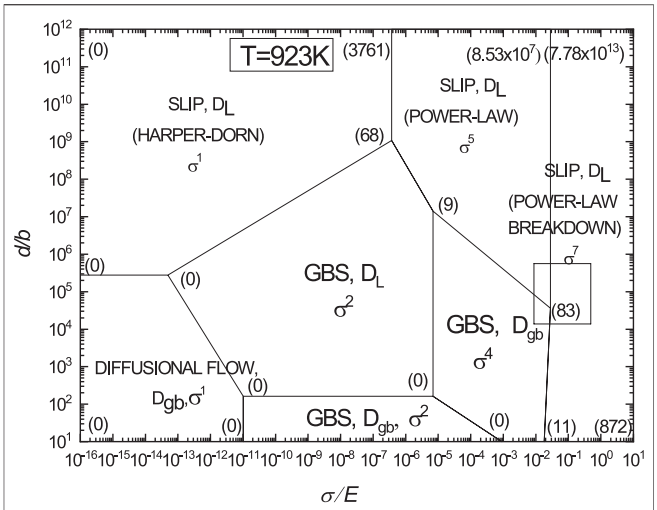

FIGURE 4 | Deformation mechanism maps of Ti-6Al-4V containing dislocation count (T = 923 K).

boundary morphology after deformation were observed and characterized by a TECNAI G^{20} TEM instrument.

RESULTS AND DISCUSSION

The stress-strain curves of Ti-6Al-4V at 923 K and strain rate of 10^{-3}, 5×10^{-3}, 5×10^{-2} s^{-1} are shown in **Figure 3**. Under the above conditions, the peak stress and steady-state stress of this alloy both decreased with the declining strain rate (**Fig. 3**). At the strain rate of 5×10^{-2} s^{-1}, the stress maximized and then rapidly decreased, and the interval of the steady-state rheological stress was narrow. At this moment, the total elongation was only 460%. When the strain speed decreased, the stress maximized and then slowly declined, and the curve was typical of steady-state rheological stress. The corresponding tension rates were 735 and 790%, respectively. These results indicate that the superplastic strain rate of this alloy is sensitive to some extent, and when the strain speed drops below 5×10^{-3} s^{-1}, the sensitivity is insignificant.

The high-temperature deformation of metals can be described by the following constitutive equation (Kim et al., 2001):

$$\dot{\varepsilon}_i = A_i \left(\frac{b}{d_i}\right)^p \cdot \frac{D}{k \cdot T \cdot b^2} \cdot \left(\frac{\sigma_i}{E}\right)^n, \quad (1)$$

where A_i, n, and p are material constants, σ_i is the stress, $\dot{\varepsilon}_i$ is the steady-state strain rate, E is Young's modulus, d_i is the grain size, b is the Burgers vector, and D is the diffusion coefficient (D_L is the lattice diffusion coefficient; D_{gb} is the crystal boundary diffusion coefficient).

The internal dislocation root count of unit crystal grains can be computed as follows (Cao et al., 2008):

$$n_i = 2[(1-\nu) \cdot \pi \cdot d_i \cdot \tau_i] / (Gb), \quad (2)$$

where n_i is the internal dislocation root count, ν is Poisson's ratio, and τ_i is the shear stress (MPa) in which $\tau_i = 0.5\sigma_i$. **Equation 1** is the constitutive equation about the high-temperature deformation of metal materials; **Eq. 2** is the dislocation control model of metal materials during superplastic deformation. **Equation 2** was mathematically transformed, and the dislocation count ni was introduced into **Eq. 1**, forming the deformation mechanism maps containing the dislocation count. Based on the experimental data in **Figure 3**, **Eqs. 1, 2** were solved; thereby, the RWS deformation mechanism maps of crystal grain sizes with dislocation count are plotted in **Figure 4**, with module compensation stress as X-axis and Burgers vector compensation as Y-axis. The physical parameters used in the calculation are listed in **Table 1**.

TABLE 1 | Physical parameters of Ti-6Al-4V alloys (Reca and Libanati, 1968; Stowell et al., 1984).

b = 2.95 × 10^{-10} m	**E = 2.87 × 10^{45} MPa**	**ν = 0.34**	**k = 1.38 × 10^{-23} J/K**
$D_{L\ 923K}$ = 3.01 × 10^{-17} m^2 s^{-1}		$D_{gb\ 923K}$ = 8.5 × 10^{-12} m^2 s^{-1}	

TABLE 2 | Calculated results of Ti-6Al-4V alloy after superplastic tensile tests.

T /K	(d/b)×10^{-7}	(σ/E)×10^4	$\dot{\varepsilon}$/(10^{-4}·s^{-1})
923	11.6–8.3	11.9–82.9	50–500

The normalized grain size with Burgers vector compensation ((d/b)×10^{-7}) and the normalized flow stress with modulus compensation ((σ/E)×10^4) of Ti-6Al-4V during superplastic tensile tests were calculated (**Table 2**).

According to **Figure 4** and **Table 2**, the superplastic deformation mechanism of Ti-6Al-4V at 923 K fell within the dislocation polygons of (8.53 × 10^7) (3,761) (68) (9) (83), (8.53×10^7) (7.78 × 10^{13}) (872) (11) (83), and (9) (0) (0) (11) (83) (the area surrounded by three sets of values). With an increase in strain rate, the superplastic deformation

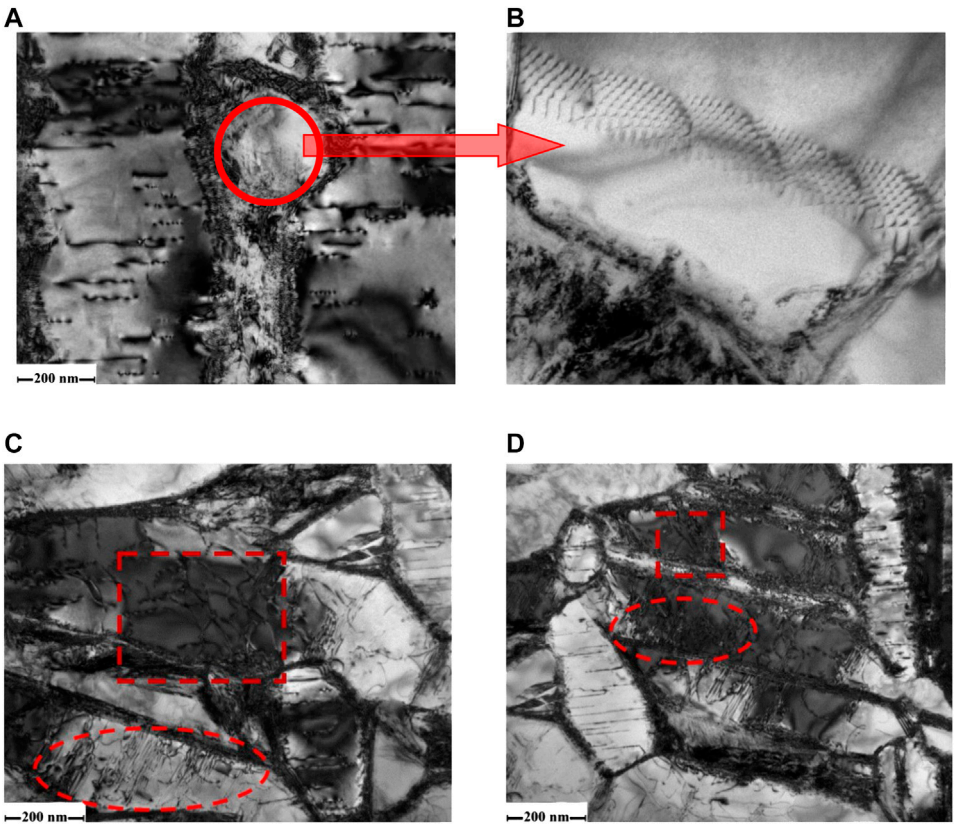

FIGURE 5 | TEM images of Ti-6Al-4V under the same superplastic tensile conditions. **(A,B)** $10^{-3}s^{-1}$; **(C)** 5×10^{-3} s^{-1}; **(D)** 5×10^{-2} s^{-1}.

mechanism transited from the dislocation-controlled grain boundary slip with a stress index of 4 to the dislocation glide with a stress index of 5 and 7, and the grain sizes during deformation affected the stress index *n*. Thus, it can be predicted from the deformation mechanism maps involving dislocation count that the superplastic deformation mechanisms of this alloy under the testing conditions were all affected by dislocation movement.

Figure 5 shows the TEM images of Ti-6Al-4V under different superplastic tensile conditions. At the strain rate of 10^{-3} s^{-1}, grain boundary deformation occurred during the superplastic tension of this alloy, and abundant irregular dislocations were formed around grain boundaries (**Figure 5A**), but the intracrystalline dislocations were arranged regularly (**Figure 5B**). With an increase in strain rate, the dislocation count gradually increased, the dislocation motion was intensified, and the dislocation slip was significant (**Figures 5C,D**), but no regular distribution, as shown in **Figure 5A**, was found. The above TEM images are consistent with the R-W-S deformation mechanism maps in **Figure 4**.

The superplastic deformation mechanism of Ti-6Al-4V at 923 K transited from dislocation-controlled grain boundary slip to dislocation glide along with an increase in strain rate. This is because the superplastic deformation of metal materials is essentially a synergy between dynamic softening mechanism and hardening mechanism, and the dynamic softening mechanism is the key factor that ensures the stable superplasticity of materials. As for Ti-6Al-4V, the softening mechanism of its superplastic tension is mainly dynamic recrystallization and recovery (Hiroaki et al., 2017). Owing to the low temperature, dislocation glide started firstly, and along with the superplastic tension, dislocation tangling occurred after the dislocation motion reached a certain extent. According to the first law of thermodynamics, the arrangement of the intertwined dislocations gradually became regular, and energy slowly dropped to the steady state, which induced recrystallization (Matsumoto et al., 2013). The proceeding of the above processes depends on appropriate dynamic conditions. Thus, the dynamic condition of this alloy at slow tension speed (10^{-3} s^{-1}) was sufficient, the irregular dislocation motion gradually turned into regular arrangement

TABLE 3 | Results of *m* and tension rate δ of Ti-6Al-4V at 923 K and different tension speeds.

Temperature *T*, K	Initial strain rate $\dot{\varepsilon}$, s^{-1}	Strain rate sensitivity exponent *m*	Tension to failure δ, %
923	10^{-3}	0.52	790
923	5×10^{-3}	0.51	735
923	5×10^{-2}	0.46	460

(**Figures 5A,B**), and the softening mechanism was the dislocation-controlled grain boundary slip (**Figure 4**). The strain rate sensitivity index m of this alloy calculated as m=(ln (1+δ))/(2 + ln (1+δ)) was 0.52 (**Table 3**). Together with the macroscopic mechanical property testing in **Figure 3**, it was known that the tension rate δ maximized to 790% and the steady-state flow stress was low. At a large strain rate (5×10^{-3} and $5 \times 10^{-2}\ s^{-1}$), the dislocation motion was still significant (**Figures 5C,D**), and due to the shortened superplastic deformation time, no regular tube-like arrangement was found, and the softening mechanism was controlled by dislocation glide and the stress index rose. At the strain rate of $5 \times 10^{-2}\ ^{-1}$, the interval of steady-state rheological stress on the stress-strain curves was significantly shortened, the peak stress and steady-state stress both significantly increased, the strain rate sensitivity index m was 0.46 (**Table 3**), and the tension rate dropped by 490%. The above results also validate that the deformation mechanisms predicted by the R-W-S deformation mechanism maps are very accurate.

CONCLUSION

During the superplastic tensile deformation of Ti-6Al-4V at low temperature (923 K) and 10^{-3}, 5×10^{-3}, or $5 \times 10^{-2}\ s^{-1}$, the tension δ and strain rate sensitivity index m both rose with the decrease in tension speed and δ maximized to 790% at $10^{-3}\ s^{-1}$. Through mathematics modeling, the unit dislocation count was introduced into the R-W-S deformation mechanism map, and a new deformation mechanism map involving the dislocation count was plotted. Thereby, the mechanism of deformation of this alloy 923 K was predicted. Owing to the low temperature, the dislocation movement significantly impacted the softening effect of this alloy during superplastic deformation. Together with microstructure characterization, it was validated that as the strain rate increases from 10^{-3} to $5 \times 10^{-2}\ s^{-1}$, the deformation mechanism transited from dislocation-controlled grain boundary slip to dislocation glide, and the stress index increased.

DATA AVAILABILITY STATEMENT

The original contributions presented in the study are included in the article/Supplementary Material; further inquiries can be directed to the corresponding author.

AUTHOR CONTRIBUTIONS

CL, XW, and LC conceived of and designed the experiments; XW and CL carried out the experiments; FL, SZ, HL, and HZ analyzed the data; CL and GZ wrote the article.

FUNDING

This research was funded by the Liaoning provincial department of finance (No. LQGD2017024), National Natural Science Foundation (No. 51805335), and Liaoning Natural Science Guidance Plan (20180550998).

REFERENCES

Cao, F. R., Ding, H., Li, Y. L., Zhao, W. J., Guo, Y. L., and Gui, J. Z. (2008). Theoretical predicati on of dislocation-included high-temperature deformation mechanism maps for duplex magnesium lithium alloys. *J. Mater. Metall.* 7, 206–210. doi:10.14186/j.cnki.1671-6620.2008.03.008

Hiroaki, M., Takuro, N., Vincent, V., and Vanessa, V. (2017). Superplastic property of the Ti–6Al–4V alloy with ultrafine-grained heterogeneous microstructure. *Adv. Eng. Mater.* 20, 1. doi:10.1002/adem.201700317

Kim, W. J., Chung, S., Chung, C., and Kum, D. (2001). Superplasticity in thin magnesium alloy sheets and deformation mechanism maps for magnesium alloys at elevated temperatures. *Acta Mater.* 49, 3337–3345. doi:10.1016/S1359-6454(01)00008-8

Li, X., Guo, G., Xiao, J., Song, N., and Li, D. (2014). Constitutive modeling and the effects of strain-rate and temperature on the formability of Ti–6Al–4V alloy sheet. *Mater. Des.* 55, 325–334. doi:10.1016/j.matdes.2013.09.069

Matsumoto, H., Bin, L., and Lee, S. (2013). Frequent occurrence of discontinuous dynamic recrystallization in Ti-6Al-4V alloy with α' martensite starting microstructure. *Metall. Mater. Trans.* 44, 3245–3260. doi:10.1007/s11661-013-1655-5

Meng, B., Fu, M. W., and Shi, S. Q. (2016). Deformation behavior and microstructure evolution in thermal-aided mesoforming of titanium dental abutment. *Mater. Des.* 89, 1283–1293. doi:10.1016/j.matdes.2015.10.105

Reca, N. E., and Libanati, C. M. (1968). Autodifusion de titanio beta y hafnio beta Self-diffusion in β-titanium and β-hafniumAutodiffusion du titane beta et de l'hafnium betaSelbstdiffusion in β-titan und β-hafnium. *Acta. Met.* 16, 1297–1305. doi:10.1016/0001-6160(68)90010-2

Shahmir, H., Naghdi, F., Pereira, P., Huang, Y., and Langdon, T. G. (2018). Factors influencing superplasticity in the Ti-6Al-4V alloy processed by high-pressure torsion. *Mater. Sci. Eng. A.* 718, 198–206. doi:10.1016/j.msea.2018.01.091

Stowell, M. J., Livesey, D. W., and Ridley, N. (1984). Cavity coalescence in superplastic deformation. *Acta Metall.* 32, 35–42. doi:10.1016/0001-6160(84)90199-8

Vanderhasten, M., Rabet, L., and Verlinden, B. (2007). Deformation mechanisms of Ti-6Al-4V during tensile behavior at low strain rate. *J. Mater. Eng. Perform.* 16, 208–212. doi:10.1007/s11665-007-9033-3

Zhang, W., Ding, H., Pereira, P., Huang, Y., and Langdon, T. G. (2018). Grain refinement and superplastic flow in a fully lamellar Ti-6Al-4V alloy processed by high-pressure torsion. *Mater. Sci. Eng. A.* 732, 398–405. doi:10.1016/j.msea.2018.07.010

Zhang, W., Ding, Hua., Cai, Minghui., Yang, Wenjing., and Li, Jizhong. (2018). Ultra-grain refinement and enhanced low-temperature superplasticity in a friction stir-processed Ti-6Al-4V alloy. *Mater. Sci. Eng. A.* 727, 90–96. doi:10.1016/j.msea.2018.03.009

Zhou, Ge., Chen, Lijia., Liu, Lirong., Liu, Haijian., Peng, Heli., and Zhong, Yiping. (2018). Low-temperature superplasticity and deformation mechanism of Ti-6Al-4V alloy. *Materials* 11, 1212. doi:10.3390/ma11071212

Conflict of Interest: The authors declare that the research was conducted in the absence of any commercial or financial relationships that could be construed as a potential conflict of interest.